Communications in Applied and Industrial Mathematics,
ISSN 2038-0909, e-441
DOI: 10.1685/journal.caim.441

Medical image registration using compactly supported functions

Alessandra De Rossi

Dipartimento di Matematica "Giuseppe Peano"
Università degli Studi di Torino, Italy
alessandra.derossi@unito.it

Communicated by Giorgio Fotia

Abstract

In this paper we consider landmark-based image registration using radial basis function interpolation schemes. More precisely, we analyze some landmark-based image transformations defined by means of compactly supported radial basis functions, namely multivariate Wendland's and Gneiting's functions. The latter, as far as we know, have never been used in this context. Comparisons of the two transformations are given. Numerical experiments performed on test examples show better accuracy of Gneiting's ones in some cases. Finally, an application of compactly supported transformations to real medical images is also considered.

Keywords: landmark-based image transformations, scattered data interpolation, radial basis functions, Wendland's functions, Gneiting's functions.

AMS subject classification: 65D05, 65D07, 68U10.

1. Introduction.

Image registration is an important challenging topic in image processing. It consists mainly in finding a suitable transformation between two images (or image data), called *source* and *target images*, taken either at different times or from different sensors or viewpoints. The scope is to determine a transformation such that the transformed version of the source image is similar to the target one. There is a large number of applications demanding image registration, including astronomy, biology, computer vision, genetics, physics, medicine, robotics, to name a few. For an overview, see e.g. [1–9] and references therein. In medicine, for example, registration is required for combining different modalities (such as X-ray, computer tomography (CT), magnetic resonance imaging (MRI) and positron emission tomography (PET) images), monitoring of diseases, treatment validation,

Received on November 27th, 2012. Accepted on May 9th, 2013. Published on August 8th, 2013.

comparison of the patient's data with anatomical atlases, and radiation therapy. In particular, the *landmark-based image registration* process is based on two finite sets of landmarks, i.e. sparse data points located on images, usually not uniformly distributed, where each landmark of the source image has to be mapped onto the corresponding landmark of the target image (see [4–6]). The landmark-based registration problem can be formulated in the context of multivariate scattered data interpolation, and solved by different techniques, among which radial basis functions (RBFs) play a preminent role (see, e.g., [10,11]). The use of RBF transformations, in particular of the thin plate splines, for point-based image registration was first proposed by Bookstein [12], and it is still common (see [13,14] and the software package MIPAV [15]).

Since using globally supported RBFs, as for example the thin plate spline or the Gaussian, a single landmark pair change may influence the whole registration result, in the last decade several methods have been presented to circumvent this disadvantage, such as Wendland's compactly supported radial basis functions (CSRBFs) [16], elastic body splines (EBSs) [17], the modified inverse distance weighted method (IDWM) [18, 19], and a spline method [20,21]. These interpolation techniques, giving rise to compactly supported or local mappings, handle well locally deformed images. Moreover, they are in general stable and the computational effort to determine transformations is low and, therefore, also a large number of landmarks can be used.

In this paper we focus on properties and performances of CSRBFs. In particular, we consider in this context compactly supported transformations defined by means of Wendland's and Gneiting's functions (see [10,11,22]).

Numerical experiments point out differences in accuracy and smoothness of the considered methods. As far as we know, the family of compactly supported radial basis functions of Gneiting has never been used in the registration context, but the results presented in this paper turn out to be very promising.

The paper is organized as follows. Section 2 introduces the landmark-based registration problem. In Section 3 Wendland's and Gneiting's compactly supported functions are briefly presented to define compactly supported transformations. Section 4 contains several numerical results obtained in some test and real examples: special emphasis is devoted to comparing accuracy of the two CSRBF schemes. Finally, Section 5 is devoted to conclusions and future work.

DOI: 10.1685/journal.caim.441

2. The landmark based registration problem.

For simplicity, in this section and in the following, we limit the presentation to the $2D$ case, but all definitions can be easily extended to the $3D$ one.

Let $\mathcal{S}_N = \{\mathbf{x}_j \in \mathbb{R}^2, j = 1, 2, \ldots, N\}$ be a given set of landmarks in the source image S and let $\mathcal{T}_N = \{\mathbf{t}_j \in \mathbb{R}^2, j = 1, 2, \ldots, N\}$ be the given set of corresponding landmarks in the target image T. The registration problem reads as follows.

Problem 2.1. *Let the landmark sets $\mathcal{S}_N$ and $\mathcal{T}_N$ be given. Find a transformation $\mathbf{F} : \mathbb{R}^2 \to \mathbb{R}^2$ within a suitable space $\mathcal{F}$ of admissible functions, such that*

$$\mathbf{F}(\mathbf{x}_j) = \mathbf{t}_j, \qquad j = 1, 2, \ldots, N. \tag{1}$$

Each coordinate F_k of the transformation function is calculated separately, i.e. the interpolation problem $F_k : \mathbb{R}^2 \to \mathbb{R}$ is solved for each $k = 1, 2$, with the corresponding conditions

$$F_k(\mathbf{x}_j) = t_{jk}, \qquad j = 1, 2, \ldots, N. \tag{2}$$

In order to have a class of basis functions that generate non-singular interpolation matrices for any set of distinct points, we introduce the concept of strictly positive definite functions [10]. We suppose that the interpolant $F_k : \mathbb{R}^2 \to \mathbb{R}$ has the form

$$F_k(\mathbf{x}) = \sum_{j=1}^{N} c_{jk} \Psi(\mathbf{x} - \mathbf{x}_j), \tag{3}$$

c_j being the coefficients to be found. A necessary condition to have unique solvability of the interpolation problem is given by the following result [10].

Theorem 2.1. *The interpolation problem (2), where F_k is of the form (3), has a unique solution if the function Ψ is strictly positive definite on $\mathbb{R}^2$, that is*

$$\sum_{i=1}^{N} \sum_{j=1}^{N} c_i c_j \Psi(\boldsymbol{x}_i - \boldsymbol{x}_j) > 0, \tag{4}$$

for any N pairwise different points $\boldsymbol{x}_1, \boldsymbol{x}_2, \ldots, \boldsymbol{x}_N \in \mathbb{R}^2$, and $\boldsymbol{c} = [c_1, c_2, \ldots, c_N]^T \in \mathbb{R}^N$, $\boldsymbol{c} \neq \boldsymbol{0}$.

Moreover, we remark that Theorem 2.1 is also satisfied for a strictly conditionally positive definite function Ψ of order v if the quadratic form (4) holds and

$$\sum_{i=1}^{N} c_i p(\mathbf{x}_i) = 0, \tag{5}$$

for any polynomial p of degree at most $v-1$.

3. Compactly supported radial basis functions.

In this section we consider some of the most popular families of CSRBFs, Wendland's and Gneiting's functions (see [10,11,22]). Wendland's functions have been introduced in image registration context with the motivation that their influence around a landmark is limited, in 2D and 3D images on a circle or a sphere, respectively [16]. This property allows us the registration of medical images where changes occur only locally. Here we also propose the use of Gneiting's functions, since they give better accuracy results in some cases (see [10]).

In this paper we limit ourselves to list the explicit forms of these CSRBF families on $\mathbb{R}^2$. They are all strictly positive definite and radial. Non-experts or interested readers could find a complete presentation of their construction and properties in [10].

3.1. *Wendland's functions.*

Since Wendland's functions are compactly supported, the interpolation matrices can be made sparse by appropriately scaling the support of the basic function. In the following we can consider only Wendland's functions depending on a shape parameter $c \in \mathbb{R}^+$. We list some of the most commonly used functions in $\mathbb{R}^2$ along with their degree of smoothness, that is

$$\begin{array}{ll} \varphi_{2,0}(r) \doteq (1-cr)_+^2\,, & \mathrm{C}^0 \\ \varphi_{2,1}(r) \doteq (1-cr)_+^4\,(4cr+1)\,, & \mathrm{C}^2 \\ \varphi_{2,2}(r) \doteq (1-cr)_+^6\,\left(35(cr)^2+18cr+3\right), & \mathrm{C}^4 \\ \varphi_{2,3}(r) \doteq (1-cr)_+^8\,\left(32(cr)^3+25(cr)^2+8cr+1\right), & \mathrm{C}^6 \end{array} \tag{6}$$

where r is the Euclidean distance in $\mathbb{R}^2$. We remark that the functions $\varphi_{2,k}$, $k=0,1,2,3$, are strictly positive definite and radial on $\mathbb{R}^m$, for $m \leq 3$ (see [11]).

DOI: 10.1685/journal.caim.441

Referring to the image registration context we can define Wendland's transformations in the following way:

Definition 3.1. Given a set of source landmark points $\mathcal{S}_N = \{\mathbf{x}_j \in \mathbb{R}^2, j = 1, 2, \ldots, N\}$, with associated the corresponding set of target landmark points $\mathcal{T}_N = \{\mathbf{t}_j \in \mathbb{R}^2, j = 1, 2, \ldots, N\}$, a *Wendland's transformation* $\mathbf{W} : \mathbb{R}^2 \to \mathbb{R}^2$ is such that each its component

$$W_k : \mathbb{R}^2 \to \mathbb{R}, \qquad k = 1, 2, \tag{7}$$

assumes the following form

$$W_k(\mathbf{x}) = W_k(x_1, x_2) = \sum_{j=1}^{N} c_{jk} \varphi_{2,h}(||\mathbf{x} - \mathbf{x}_j||_2), \tag{8}$$

with $\mathbf{x} = (x_1, x_2)$ and $\mathbf{x}_j = (x_{j1}, x_{j2}) \in \mathbb{R}^2$.

From Definition 3.1 it follows that the transformation function $W_k : \mathbb{R}^2 \to \mathbb{R}$ is calculated for each $k = 1, 2$, and the coefficients c_{jk} are to be obtained by solving two systems of linear equations.

3.2. *Gneiting's functions.*

Starting with Wendland's functions and applying the turning bands operator, Gneiting in 2002 obtained a family of compactly supported functions [22]. Following [10], we can start with a function φ_s that is strictly positive definite and radial on $\mathbb{R}^s$ for $s \geq 3$, and applying the turning bands operator results

$$\varphi_{s-2}(r) = \varphi_s(r) + \frac{r\varphi_s'(r)}{s-2}, \tag{9}$$

which is strictly positive definite and radial on $\mathbb{R}^{s-2}$. For example, starting with the Wendland function $\varphi_{4,1}(r) = (1-r)_+^{l+1}[(l+1)r+1]$ and applying the turning bands operator we obtain the functions

$$\tau_{2,l}(r) = (1-r)_+^l \left(1 + lr - \frac{(l+1)(l+4)}{2} r^2\right), \tag{10}$$

which are strictly positive definite and radial on $\mathbb{R}^2$ provided $l \geq 7/2$. We list some specific functions from this family for various choices of l. All of the functions are in $\mathrm{C}^2(\mathbb{R})$.

$$\begin{aligned}
\tau_{2,7/2}(r) &\doteq (1-cr)_+^{7/2} \left(1 + \tfrac{7}{2}cr - \tfrac{135}{8}(cr)^2\right), && \mathrm{C}^2 \\
\tau_{2,5}(r) &\doteq (1-cr)_+^{5} \left(1 + 5cr - 27(cr)^2\right), && \mathrm{C}^2 \\
\tau_{2,15/2}(r) &\doteq (1-cr)_+^{\frac{15}{2}} \left(1 + \tfrac{15}{2}cr - \tfrac{391}{8}(cr)^2\right), && \mathrm{C}^2 \\
\tau_{2,12}(r) &\doteq (1-cr)_+^{12} \left(1 + 12cr - 104(cr)^2\right). && \mathrm{C}^2
\end{aligned} \tag{11}$$

With regard to the image registration context we can define Gneiting's transformations as follows.

Definition 3.2. Given a set of source landmark points $\mathcal{S}_N = \{\mathbf{x}_j \in \mathbb{R}^2, j = 1, 2, \ldots, N\}$, with associated the corresponding set of target landmark points $\mathcal{T}_N = \{\mathbf{t}_j \in \mathbb{R}^2, j = 1, 2, \ldots, N\}$, a *Gneiting's transformation* $\mathbf{G} : \mathbb{R}^2 \to \mathbb{R}^2$ is such that each its component

$$G_k : \mathbb{R}^2 \to \mathbb{R}, \qquad k = 1, 2, \tag{12}$$

assumes the following form

$$G_k(\mathbf{x}) = G_k(x_1, x_2) = \sum_{j=1}^{N} c_{jk} \tau_{2,l}(||\mathbf{x} - \mathbf{x}_j||_2), \tag{13}$$

with $\mathbf{x} = (x_1, x_2)$ and $\mathbf{x}_j = (x_{j1}, x_{j2}) \in \mathbb{R}^2$.

As for Wendland's transformation, from Definition 3.2 it follows that the transformation function $G_k : \mathbb{R}^2 \to \mathbb{R}$ is calculated for each $k = 1, 2$, and the coefficients c_{jk} are to be obtained by solving two systems of linear equations.

We point out that in scattered data interpolation, in some cases, accuracy achieved using Gneiting's functions is better than that obtained using Wendland's functions (see [10]).

4. Numerical experiments.

In this section, we compare the performances of the above methods when they are applied to give image transformations. In particular, we consider transformations defined by means of bivariate Wendland's and Gneiting's functions, both of regularity C^2.

In order to test the two different CSRBF interpolation schemes, we obtained several numerical results on some test cases, which simulate typical medical cases where image portions scale or shift. These image portions represent rigid objects embedded in elastic material changing their position or form. The approach we propose can cope with local differences between corresponding images. In general these differences may be caused by the physical deformation of human tissue due to surgeries or pathological processes such as tumor growth or tumor resection. However, the aim is here to determine a transformation function, which connects the points of the source and target images, so that the target image is affected by the slightest possible deformation. The comparison is made also analyzing the behaviour of the root mean squares error (RMSE). Root mean squares

DOI: 10.1685/journal.caim.441

error is found computing the distances between the displacements of grid points $\mathbf{x} \in \mathcal{X}$ and the values obtained by the transformations. It assumes the following form

$$\text{RMSE} = \sqrt{\frac{\sum_{\mathbf{x}\in\mathcal{X}} \|\mathbf{x} - \mathbf{F}(\mathbf{x})\|_2^2}{\sum_{\mathbf{x}\in\mathcal{X}} 1}}, \tag{14}$$

where $\|\cdot\|_2$ is the Euclidean norm.

Here, for brevity, we refer to two test examples given in [17]. Finally, we present some experimental results obtained by applying Wendland's and Gneiting's transformations to real image data. More precisely, we consider two X-ray images of the cervical of an anonymous patient taken at different times. The considered real example is very similar to that taken by Modersitzki in [5].

4.1. *Test examples: circle expansion and contraction.*

In this subsection we consider two opposite radial transformations, that is, the expansion and the contraction of a circle (see Figure 1). They may offer very schematic models for the growing and the resection of a tumor in surrounding elastic brain tissue. In these models (given in [17]) the outer circle corresponds to the skull bone, which is assumed to be rigid. The inner circle represents the boundary of the tumor, whereas the space between the inner and the outer circle is assumed to be filled with elastic material, which corresponds to brain tissue.

Images are registered using 20 equidistant landmarks placed on the inner circle and, to prevent an overall shift, also 40 quasi–landmarks, i.e. landmarks at invariant positions, at the outer circle in the source and target images. These point-landmarks, shown in Figure 1 for the circle expansion (left) and the circle contraction (right), are marked by a circle ($\circ$) and a star ($\star$), respectively.

In Tables 1 and 2 we report the root mean squares errors obtained by using Wendland's transformation defined by means of the function $\varphi_{2,1}$, called for brevity $W_{2,1}$, and Gneiting's transformations given by the functions $\tau_{2,7/2}$ and $\tau_{2,5}$, called $G_{2,7/2}$ and $G_{2,5}$, respectively. Values of shape parameters are chosen equal to 0.1 for all transformations. We point out that in general CSRBF transformations give less deformations, and therefore registration results are better, if we use small values for the parameters, say $c \in [0.01, 0.3]$.

A comparison of RMSEs points out that errors for Gneiting's transformation, for $l = 7/2$, are approximatively a half than those obtained using

Table 1. Circle expansion - 20 landmarks: RMSEs for $c = 0.1$.

$W_{2,1}$	$G_{2,7/2}$	$G_{2,5}$
$9.1226\text{E}-2$	$4.0166\text{E}-2$	$9.4606\text{E}-2$

Table 2. Circle contraction - 20 landmarks: RMSEs for $c = 0.1$.

$W_{2,1}$	$G_{2,7/2}$	$G_{2,5}$
$9.1792\text{E}-2$	$5.2041\text{E}-2$	$7.9795\text{E}-2$

Wendland's transformation, while for $l = 5$ Gneiting's transformation is comparable with the Wendland's one.

It is well known that also shape and smoothness of the transformed grids may be relevant to compare different transformations. To this aim in the Figures 2 and 3 we present registration results obtained by the two CSRBFs interpolation methods. Here we observe significant differences. Registration result involving interpolation scheme $W_{2,1}$ is worse than that obtained with Gneiting's transformation $G_{2,7/2}$. In fact, for both circle expansion and contraction, Gneiting's transformation produces a visibly smooth grid, while images are visibly deformed when Wendland's transformation is used. This behaviour is observed in all the test cases analyzed during the experimental phase of the work.

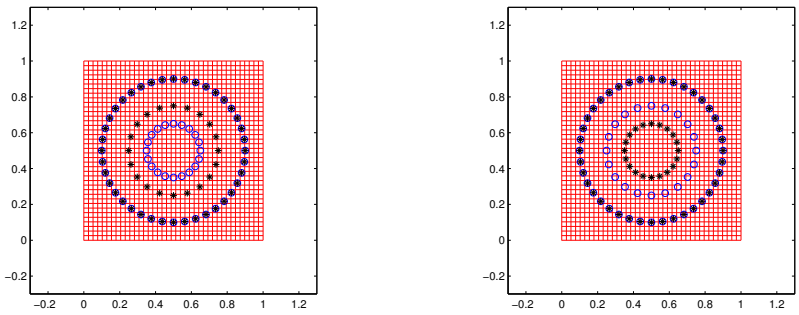

Figure 1. Circle expansion (left) and contraction (right): source and target landmarks.

4.2. *An application to medical images.*

In this subsection we present some experimental results obtained by applying Wendland's and Gneiting's transformations to real image data. More precisely, we consider two X-ray images of the cervical of an anonymous patient taken at different times. The considered real example is very

DOI: 10.1685/journal.caim.441

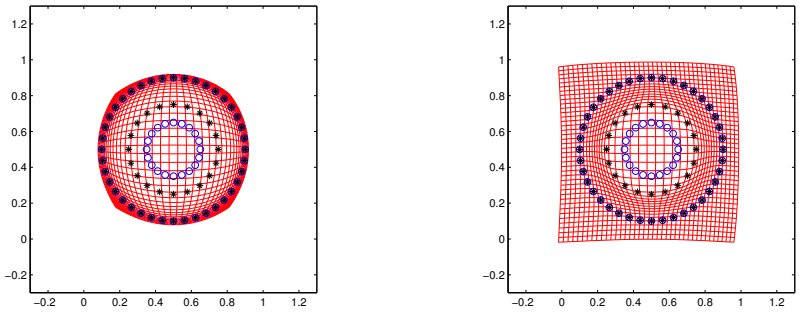

Figure 2. Circle expansion: registration results obtained by using Wendland's (left) and Gneiting's transformations (right).

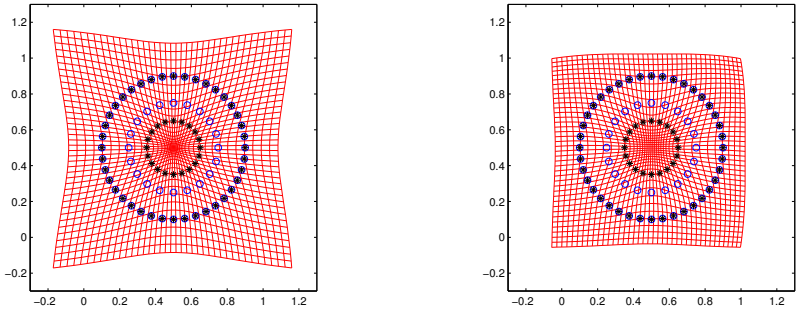

Figure 3. Circle contraction: registration results obtained by using Wendland's (left) and Gneiting's transformations (right).

similar to that given by Modersitzki in [5]. In Figure 4 we show the two images along with landmarks and quasi-landmarks, setting on the left the source image and on the right the target one. The size of both images is 512×512 pixels. In particular, within each of the two images we have manually selected 6 landmarks and, moreover, to fix transformation and prevent an overall shift, we have added 12 quasi-landmarks on the boundaries of the source and target images.

Each result in Figure 5 represents a registered image, obtained using Wendland's $W_{2,1}$ and Gneiting's $G_{2,7/2}$ transformations, respectively. For both transformations we have used the parameter value $c = 0.1$. We remark that Gneiting's registration result compares well with Wendland's one.

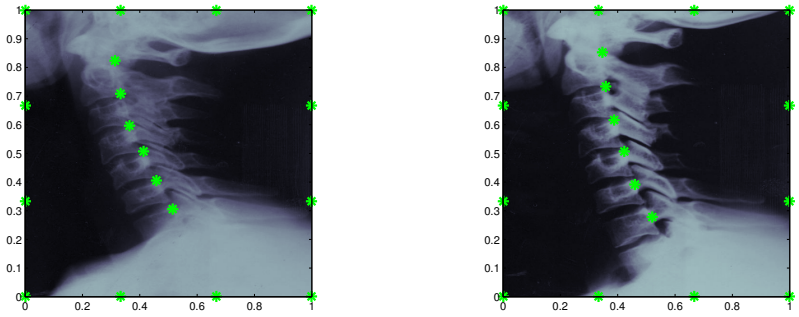

Figure 4. Source and target cervical images with landmarks and quasi-landmarks (left to right).

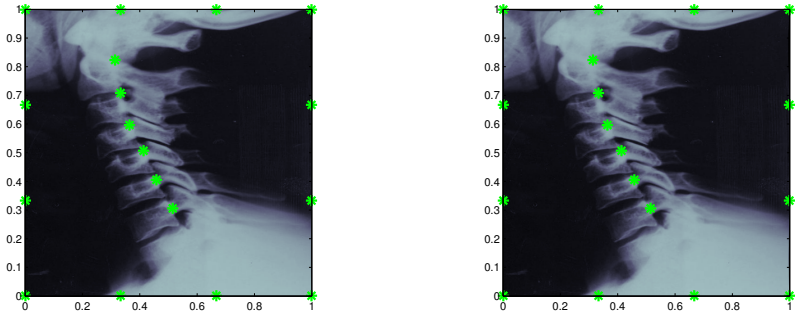

Figure 5. Real-life case: registration results obtained by Wendland's (left) and Gneiting's (right) transformations.

5. Conclusions and future work.

We compared some well established compactly supported interpolation methods, such as Wendland's and Gneiting's functions. To this aim, we briefly recalled the two interpolation schemes. For the first time, as far as we know, we proposed in the image registration context the use of compactly supported radial basis Gneiting's functions, which perform well in scattered data interpolation when compared with other schemes. Gneiting's transformations, when compared with Wendland's ones, perform better in many test cases and examples. In the real case presented in this paper, Gneiting's and Wendland's transformations are comparable. We point out that this investigation is only a first step to include Gneiting's interpolants in the set of functions to be used in landmark-based image registration. The next step, which is still a work in progress, consists in showing that

DOI: 10.1685/journal.caim.441

Gneiting's transformations preserve the topology.

Moreover, here we used interpolating transformations which accomplish an exact match of corresponding landmarks. This implicitly means that the landmark positions are exactly known. However, if we have to deal with landmark localization errors, then it would be advantageous to weaken the interpolation conditions by introducing an approximation scheme. Further investigations in this direction are still required and ongoing.

Acknowledgements.

The author thanks the anonymous referee for the valuable comments which helped to improve the quality of the paper. Moreover, the author gratefully acknowledge the support of Department of Mathematics "G. Peano", University of Turin, project "Modeling and approximation of complex systems (2010)".

REFERENCES

1. A. A. Goshtasby, *2-D and 3-D Image Registration.* Wiley, 2005.
2. J. Hajnal, D. Hill, and D. Hawkes, *Medical Image Registration.* CRC Press, 2001.
3. M. Holden, A review of geometric transformations for nonrigid body registration, *IEEE Trans. Med. Imaging*, vol. 27, pp. 111–128, 2008.
4. J. Modersitzki, *Numerical Methods for Image Registration.* Oxford Univ. Press, 2004.
5. J. Modersitzki, *FAIR: Flexible Algorithms for Image Registration, Fundam. Algorithms 6.* SIAM, 2009.
6. K. Rohr, *Landmark-Based Image Analysis, Using Geometric and Intensity Models.* Kluwer Academic Publishers, 2001.
7. O. Scherzer, *Mathematical Models for Registration and Applications to Medical Imaging.* Springer, 2006.
8. L. Zagorchev and A. A. Goshtasby, A comparative study of transformation functions for nonrigid image registration, *IEEE Trans. Image Processing*, vol. 15, pp. 529–538, 2006.
9. B. Zitová and J. Flusser, Image registration: a survey, *Image Vision Comput.*, vol. 21, pp. 977–1000, 2003.
10. G. E. Fasshauer, *Meshfree Approximation Methods with MATLAB.* World Scientific Publishers, 2007.
11. H. Wendland, *Scattered Data Approximation.* Cambridge Univ. Press, 2005.
12. F. L. Bookstein, Principal warps: thin-plate splines and the decomposi-

tion of deformations, *IEEE Trans. Pattern Anal. Mach. Intell.*, vol. 11, pp. 567–585, 1989.

13. B. Quatember, M. Mayr, W. Recheis, S. Demertzis, G. Allasia, R. Cavoretto, A. De Rossi, and E. Venturino, Geometric modelling and motion analysis of the epicardial surface of the heart, *Math. Comput. Simulation*, vol. 81, pp. 608–622, 2010.
14. B. Quatember, M. Mayr, W. Recheis, S. Demertzis, G. Allasia, R. Cavoretto, A. De Rossi, and E. Venturino, Development of an accurate method for motion analyses of the heart wall based on medical imagery, in *Computer Aided Systems Theory – EUROCAST 2011, LNCS 6928* (R. Moreno-Díaz et al., ed.), pp. 248–255, Springer-Verlag, 2012.
15. MIPAV, *Medical Image Processing, Analysis and Visualization.* software package.
16. M. Fornefett, K. Rohr, and H. S. Stiehl, Radial basis functions with compact support for elastic registration of medical images, *Image Vision Comput.*, vol. 19, pp. 87–96, 2001.
17. J. Kohlrausch, K. Rohr, and H. Stiehl, A new class of elastic body splines for nonrigid registration of medical images, *J. Math. Imaging Vision*, vol. 23, pp. 253–280, 2005.
18. R. Cavoretto, A. De Rossi, B. Quatember, W. Recheis, M. Mayr, and S. Demertzis, A local IDW transformation algorithm for medical image registration, in *AIP Conf. Proc. 1048* (T. E. Simos et al., ed.), pp. 970–973, Melville, 2008.
19. R. Cavoretto, A. De Rossi, and B. Quatember, Landmark-based registration using a local radial basis function transformation, *J. Numer. Anal. Ind. Appl. Math.*, vol. 5, pp. 141–152, 2011.
20. G. Allasia, R. Cavoretto, A. De Rossi, B. Quatember, W. Recheis, M. Mayr, and S. Demertzis, Radial basis functions and splines for landmark-based registration of medical images, in *AIP Conf. Proc. 1281* (T. E. Simos et al., ed.), pp. 716–719, Melville, 2010.
21. G. Allasia, R. Cavoretto, and A. De Rossi, A class of spline functions for landmark-based image registration, *Math. Meth. Appl. Sci.*, vol. 35, pp. 923–934, 2012.
22. T. Gneiting, Compactly supported correlation functions, *Journal of Multivariate Analysis*, vol. 83, pp. 493–508, 2002.